The Astronomical Journal, 153:155 (9pp), 2017 April https://doi.org/10.3847/1538-3881/aa5daa

Temporary Capture of Asteroids by an Eccentric Planet

A. Higuchi[1] and S. Ida[2]
[1] Department of Earth and Planetary Sciences, Faculty of Science, Tokyo Institute of Technology, Meguro, Tokyo 152-8551, Japan
[2] Earth-Life Science Institute, Tokyo Institute of Technology, Meguro, Tokyo 152-8550, Japan
Received 2016 November 29; revised 2017 January 27; accepted 2017 January 30; published 2017 March 10

Abstract

We have investigated the probability of temporary capture of asteroids in eccentric orbits by a planet in a circular or eccentric orbit through analytical and numerical calculations. We found that, in the limit of the circular orbit, the capture probability is ∼0.1% of encounters to the planet's Hill sphere, independent of planetary mass and semimajor axis. In general, temporary capture becomes more difficult as the planet's eccentricity (e_p) increases. We found that the capture probability is almost independent of e_p until a critical value (e_p^c) that is given by ≃5 times the Hill radius scaled by the planet's semimajor axis. For $e_p > e_p^c$, the probability decreases approximately in proportion to e_p^{-1}. The current orbital eccentricity of Mars is several times larger than e_p^c. However, since the range of secular change in Martian eccentricity overlaps e_p^c, the capture of minor bodies by Mars in the past is not ruled out.

Key words: planets and satellites: formation

1. Introduction

Irregular satellites around giant planets, which are small and with elliptical and inclined orbits, are usually thought to be captured passing asteroids (e.g., Jewitt & Haghighipour 2007; Nicholson et al. 2008). The objects captured temporarily in the Hill sphere of a planet can be permanently captured by some energy loss (e.g., tidal dissipation, drag force from a circumplanetary disk when it existed, or collisions with other solid bodies in the disk). Higuchi & Ida (2016) derived conditions for temporary capture by a planet in a *circular* orbit as functions of the mass and semimajor axis of the host planet, and clarified the range of semimajor axes of field particles for prograde and retrograde capture.

Higuchi & Ida (2016) commented that the small eccentricity of Jupiter does not affect the capture probability. However, the effect of a high eccentricity like that of Mars has not been investigated. Mars has two satellites: Phobos and Deimos. Two major theories of the origin of these satellites are (1) in situ formation through accretion of impact-generated debris by a large impact inferred from the Borealis basin (e.g., Citron et al. 2015; Rosenblatt et al. 2016), and (2) capture of asteroids (e.g., Burns 1978). While the large impact model may explain the circular, non-inclined orbits of Phobos and Deimos, which is not easily explained by the capture origin, the surface characteristics of the satellites are similar to those of primitive asteroids. Spectral observations of Phobos and Deimos suggest that the material of the satellites is best modeled as primitive material, which may not be easily explained by the large impact origin (Fraeman et al. 2014). Future sample return missions, such as *Mars Moon eXploration*, will provide important clues about the Martian satellite origin. It is important to explore the possibility of the capture origin model in detail, as well as to investigate the large impact model.

In this study, we generalize our previous study to investigate the effects of orbital eccentricity of a planet on the temporary capture probability through analytical and numerical calculations. We derive the probability of temporary capture from encounters with the planet's Hill sphere as a function of planetary eccentricity e_p and mass m_p. If the encounter frequency is given by other simulations, we can evaluate the probability of temporary capture throughout the history of the solar system. Most of our analysis and orbital calculations assume planar orbits, but some calculations are done with small finite inclinations. Temporary capture is a necessary condition for permanent capture. The relation between temporary and permanent capture will be investigated in a subsequent paper.

We summarize the assumptions, basic formulation, and derivation of the analytical formulae in Section 2. We define and derive the efficiency of temporary capture in Section 3. The methods and results of numerical calculations are presented and compared with the analytical prediction in Section 4. In Section 5, we summarize the results and comment on the origin of Martian satellites.

2. Analytical Derivation of Temporary Capture Efficiency by an Eccentric Planet

We first derive analytical formulae for temporary capture by an eccentric planet. These formulae give orbital elements of the asteroids that can be captured, as functions of the mass, eccentricity, and true anomaly of the host planet. As we will show in Section 4, the analytical formulae reproduce the results obtained through numerical orbital integrations. From the analytical derivation, the intrinsic dynamics of temporary capture by an eccentric planet will be revealed.

2.1. Assumptions

Following Higuchi & Ida (2016), we split a coplanar three-body problem (Sun–planet–particle) into two independent two-body problems (Sun–particle and planet–particle). The particles are candidates that are captured by the planet to become satellites. Hereafter, we refer to particles as "asteroids," although the particles do not necessarily originate from the asteroid belt. We identify the relative velocity between the asteroid and the planet in heliocentric orbits with the satellite velocity orbiting around the planet (condition [1]) at the capture point. The capture points are assumed to be the L_1 and L_2 points (condition [2]). The distance of the points from the

planet is the Hill radius,

$$r_{\rm H} = r_{\rm p}\left(\frac{m_{\rm p}}{3M_\odot}\right)^{\frac{1}{3}} = r_{\rm p}\hat{r}_{\rm H}, \quad (1)$$

where $m_{\rm p}$ is the planet mass and $M_\odot$ is the solar mass. The instantaneous heliocentric distance is given by

$$r_{\rm p} = a_{\rm p}\frac{1-e_{\rm p}^2}{1+e_{\rm p}\cos f_{\rm p}}, \quad (2)$$

where $a_{\rm p}$, $m_{\rm p}$, $e_{\rm p}$, and $f_{\rm p}$ are semimajor axis, mass, eccentricity, and true anomaly of the planet, respectively. We also assume the geometric condition that the two elliptic orbits are touching at a capture point; the velocity vectors of the planet and the asteroid are parallel or antiparallel (condition [3]).

2.2. Conditions for Temporary Capture

We consider an asteroid and a planet in Cartesian coordinates (x, y) centered on the Sun. The x-axis is toward the perihelion of the planet's orbit and the x–y plane lies in the planet's orbital plane. Let r, a, e, and f be heliocentric distance, semimajor axis, eccentricity of the asteroid, and true anomaly, respectively.

Condition [2] reads as

$$r = a\frac{1-e^2}{1+e\cos(f+\theta)} = r_{\rm p}A_{\mp}, \quad (3)$$

where $\theta = f_{\rm p} - f$ and

$$\begin{cases} A_- = 1-\hat{r}_{\rm H} \text{ at } L_1 \\ A_+ = 1+\hat{r}_{\rm H} \text{ at } L_2. \end{cases} \quad (4)$$

The heliocentric velocity of the asteroid at capture is

$$v = \sqrt{GM_\odot\left(\frac{2}{r}-\frac{1}{a}\right)} = \sqrt{GM_\odot\left(\frac{2}{A_{\mp}r_{\rm p}}-\frac{1}{a}\right)} = v_{\rm p}\chi, \quad (5)$$

where $v_{\rm p} = \sqrt{GM_\odot/a_{\rm p}}$ and

$$\chi = \sqrt{\frac{2}{\Phi_{\rm p}A_{\mp}} - \frac{a_{\rm p}}{a}}, \quad (6)$$

$$\Phi_{\rm p} = \frac{1-e_{\rm p}^2}{1+e_{\rm p}\cos f_{\rm p}}. \quad (7)$$

Condition [1] reads as

$$\boldsymbol{v} - \boldsymbol{v}_{\rm p} = \boldsymbol{v}_{\rm s}, \quad (8)$$

where $\boldsymbol{v}$ and $\boldsymbol{v}_{\rm p}$ are heliocentric velocities of the asteroid and the planet and $\boldsymbol{v}_{\rm s}$ is the planetocentric velocity of the asteroid as a satellite at capture. The velocity of the satellite at the planetocentric distance $r_{\rm s} = r_{\rm H}$ is

$$v_{\rm s} = \sqrt{Gm_{\rm p}\left(\frac{2}{r_{\rm H}}-\frac{1}{a_{\rm s}}\right)} = v_{\rm H}\sqrt{2-\Phi_{\rm s}}, \quad (9)$$

where $a_{\rm s} = r_{\rm H}/\Phi_{\rm s}$ is the planetocentric semimajor axis of the satellite,

$$\Phi_{\rm s} = \frac{1-e_{\rm s}^2}{1+e_{\rm s}\cos f_{\rm s}}, \quad (10)$$

$$v_{\rm H} = \sqrt{\frac{Gm_{\rm p}}{r_{\rm H}}} = \sqrt{\frac{3}{\Phi_{\rm p}}}\hat{r}_{\rm H}, \quad (11)$$

and $e_{\rm s}$ and $f_{\rm s}$ are the planetocentric eccentricity and true anomaly. Since $v_{\rm H}$ is a circular velocity around the planet at the planetocentric distance $r_{\rm s} = r_{\rm H}$,

$$\nu = v_{\rm s}/v_{\rm H} = \sqrt{2-\Phi_{\rm s}} \quad (12)$$

is related to the planetocentric orbital eccentricity (which is equivalent to κ^2 appearing in Higuchi & Ida 2016); $\nu = 1$ corresponds to a circular orbit with semimajor axis $a_{\rm s} = r_{\rm H}$ and the orbit is hyperbolic for $\nu > \sqrt{2}$.

Condition [3] is expressed by $\alpha = \alpha_{\rm p}$, where α and $\alpha_{\rm p}$ are the angles between the position and velocity vectors of the asteroid and those of the planet, which are given by

$$\sin\alpha = \frac{1+e\cos(f+\theta)}{\sqrt{1+e^2+2e\cos(f+\theta)}} \quad (13)$$

$$\sin\alpha_{\rm p} = \frac{1+e_{\rm p}\cos f_{\rm p}}{\sqrt{1+e_{\rm p}^2+2e_{\rm p}\cos f_{\rm p}}}. \quad (14)$$

These angles are given geometrically, applying the law of cosines to a triangle composed of $\boldsymbol{r}$, the x axis, and the tangent line of the orbit at r. Another way to derive α using the angular momentum is found in Roy (2005).

2.3. Equation of Temporary Capture

We combine the equations describing the three conditions above, and solve for the orbital elements of temporarily captured asteroids.

2.3.1. Derivation of Heliocentric Orbital Elements for Temporary Capture

Semimajor axis. Using $\boldsymbol{v}\|\boldsymbol{v}_{\rm p}$ (condition [3]), $v_{\rm s} = \nu v_{\rm H}$ (Equation (9)), and $v = v_{\rm p}\chi$ (Equation (12)), condition [1] (Equation (8)) becomes

$$|\chi - 1| = \nu v_{\rm H}. \quad (15)$$

Substituting Equations (3), (4), and (6), into Equation (15), we obtain the heliocentric semimajor axis of the asteroid at temporary capture as

$$\frac{a}{a_{\rm p}} \equiv \bar{a}_{\rm tc} = \Phi_{\rm p}\left[\frac{2}{A_{\mp}} - (\sqrt{2-\Phi_{\rm p}} \pm \sqrt{3}\,\nu\hat{r}_{\rm H})^2\right]^{-1}. \quad (16)$$

Note that Equation (16) has four values corresponding to a combination of prograde or retrograde and L_1 or L_2. If the sign in front of $\sqrt{3}$ is "+," the temporary capture is prograde. The "−" sign represents retrograde capture. The sign in $A_{\mp}$ represents L_1-type or L_2-type (Equation (4)).

Eccentricity. The heliocentric orbital angular momentum of the asteroid is

$$h = rv\sin\alpha = \sqrt{GM_\odot a(1-e^2)}. \quad (17)$$

Substituting Equations (17) into condition [2] given by Equation (3) with $\alpha = \alpha_{\rm p}$, we obtain the heliocentric

eccentricity at temporary capture,

$$e_{\rm tc} = \sqrt{1 - \sin\alpha_{\rm p}\left[1 - \left(1 - \frac{\Phi_{\rm p}A_{\mp}}{\bar{a}_{\rm tc}}\right)\right]}. \quad (18)$$

Angle of perihelion θ. The perihelion angle at temporary capture is easily obtained from Equation (3),

$$\theta_{\rm tc} = f_{\rm p} - \mathrm{acos}(g), \quad (19)$$

$$g = \frac{\frac{\bar{a}_{\rm tc}}{\Phi_{\rm p}A_{\mp}}(1 - e_{\rm tc}^2) - 1}{e_{\rm tc}} = -e_{\rm tc}^{-1}(\cos^2\alpha_{\rm p} \mp \sin\alpha_{\rm p}\sqrt{e_{\rm tc}^2 - \cos^2\alpha_{\rm p}}), \quad (20)$$

where Equation (18) is substituted at the end.

Inclination. If the asteroid has non-zero heliocentric inclination i, the relative velocity is modified. Since the relative velocity is equal to $v_{\rm s}$,

$$\begin{aligned} v_{\rm s}^2 &= (v\cos i - v_{\rm p})^2 + v^2\sin^2 i \\ &= v_{\rm p}^2\left[\left(\frac{2}{\Phi_{\rm p}A_{\mp}} - \frac{a_{\rm p}}{a}\right) + \left(\frac{2}{\Phi_{\rm p}} - 1\right) - 2\sqrt{\frac{2}{\Phi_{\rm p}A_{\mp}} - \frac{a_{\rm p}}{a}}\sqrt{\frac{2}{\Phi_{\rm p}} - 1}\cos i\right] \\ &= v_{\rm p}^2\left[\chi^2 + \left(\frac{2}{\Phi_{\rm p}} - 1\right) - 2\chi\left(\frac{2}{\Phi_{\rm p}} - 1\right)\cos i\right], \end{aligned} \quad (21)$$

which is reduced to

$$\chi^2 + \left(\frac{2}{\Phi_{\rm p}} - 1\right) - 2\chi\sqrt{\frac{2}{\Phi_{\rm p}} - 1}\cos i = (\nu v_{\rm H})^2. \quad (22)$$

For this equation to have a solution, the inclination must satisfy

$$\sin i < \sqrt{\frac{3}{2 - \Phi_{\rm p}}}\,\nu\hat{r}_{\rm H}. \quad (23)$$

The maximum value of i for capture is obtained with $f_{\rm p} = 180^\circ$ ($\Phi_{\rm p} = 1 + e_{\rm p}$).

2.3.2. Dependence on $f_{\rm p}$ and $e_{\rm p}$

Higuchi & Ida (2016) found that capture is mostly retrograde for asteroids near the planetary orbit and prograde for those from distant orbits. We found that this property does not change for a planet in an eccentric orbit. The solutions to Equation (16) are plotted against $f_{\rm p}$ with $e_{\rm p} = 0.2$ and a Jovian mass planet for ν from $\nu = 0$ (planetocentric circular orbit case) to $\nu = \sqrt{2}$ (parabolic orbit cases) in Figures 1(a) and (b). For $f_{\rm p} = 0$, the plot shows the following:

$\bar{a} \lesssim 0.6$	:	[no capture, L_1]
$0.6\ (=\bar{a}_{\rm min}) \lesssim \bar{a} \lesssim 0.8$	:	[prograde, L_1]
$0.8 \lesssim \bar{a} \lesssim 0.85$	:	[prograde, L_1] and [retrograde, L_2]
$0.85 \lesssim \bar{a} \lesssim 1.2$	:	[retrograde, L_1, L_2]
$1.2 \lesssim \bar{a} \lesssim 1.45$	:	[retrograde, L_1] and [prograde, L_2]
$1.45 \lesssim \bar{a} \lesssim 2.9\ (=\bar{a}_{\rm max})$	:	[prograde, L_2]
$2.9 \lesssim \bar{a}$	:	[no capture, L_1]

The asteroids from these regions to the planet's Hill sphere have orbital eccentricities given by Equation (18). As seen in Figures 1(a) and (b), the boundaries of individual regions depend on $f_{\rm p}$. The planet can capture asteroids from further regions near perihelion ($f_{\rm p} = 0/360^\circ$) than near aphelion. During a planet's orbital period, the instantaneous Hill radius $r_{\rm H}$ and $v_{\rm H}$ change. At its perihelion, $v_{\rm H}$ has the largest value, so that the planet captures asteroids from distant regions that have large relative velocity. Equation (16) suggests that the range of encounters, $\bar{a}_{\rm max} - \bar{a}_{\rm min}$, increases with $m_{\rm p}$ and $e_{\rm p}$, because $\hat{r}_{\rm H} \propto m_{\rm p}^{1/3}$ and $\Phi_{\rm s} \propto e_{\rm p}$ (for $e_{\rm p}^2 \ll 1$). Numerically obtained values of $\bar{a}_{\rm max}$ and $\bar{a}_{\rm min}$ are plotted in Figure 2.

Figures 1(c) and (d) show the solutions to Equation (20) with $\nu = \sqrt{2}$ for different values of $e_{\rm p}$. For $e_{\rm p} \sim 0$, $\theta_{\rm tc}$ covers the range (0°–360°) as $f_{\rm p}$ changes from 0° to 360°. The whole range is covered for small values of $\theta_{\rm tc}$ with slight modulation. However, for $e_{\rm p}$ larger than a threshold value ($e_{\rm p}^{\rm c}$), the coverage of $\theta_{\rm tc}$ is only a part of 0°–360°. We will show that capture probability decreases with the increase in $e_{\rm p}$ when $e_{\rm p} > e_{\rm p}^{\rm c}$. Since we found that $e_{\rm p}^{\rm c}$ is largest for $\nu = \sqrt{2}$, we define the value for $\nu = \sqrt{2}$ with a given $m_{\rm p}$ as $e_{\rm p}^{\rm c}$ for $m_{\rm p}$.

2.3.3. The Dependence of $e_{\rm p}^{\rm c}$ on the Planetary Mass

The values of $e_{\rm p}^{\rm c}$ are obtained numerically, by finding the point satisfying $d\theta_{\rm tc}/df_{\rm p} = 0$. Figure 3 shows $e_{\rm p}^{\rm c}$ for four types of temporary capture for $\nu = \sqrt{2}$ as a function of $m_{\rm p}$. The dependence of $e_{\rm p}^{\rm c}$ on $m_{\rm p}$ is approximately given by $e_{\rm c} \simeq 5\hat{r}_{\rm H} \propto m_{\rm p}^{1/3}$.

In the figure, the current values of the eccentricities of eight planets of the solar system are also plotted. The bars attached to the points show the maximum variation ranges over past 10 Myr, calculated following the method developed by Ito et al. (1995) which is based on the secular perturbation theory of Laskar (1988). As we will show later, the analytically derived values of $e_{\rm p}$, beyond which the temporary capture probability drops, agree with the results obtained by numerical orbital integration. Jupiter, Saturn, and Neptune always have $e_{\rm p} < e_{\rm p}^{\rm c}$. This means that their rates of temporary capture have remained relatively high. The maximum $e_{\rm p}$ values for Venus, Earth, and Uranus are slightly higher than $e_{\rm p}^{\rm c}$ but the current values and most of the error-bar ranges of $e_{\rm p}$ are below $e_{\rm p}^{\rm c}$.

Mars, which has relatively high $e_{\rm p}$, apparently has less chance to capture asteroids with its current orbit. However, the bar of $e_{\rm p}$ for Mars shows that the Martian $e_{\rm p}$ can have values much smaller than $e_{\rm p}^{\rm c}$ during orbital variations. Mercury has never had $e_{\rm p} < e_{\rm p}^{\rm c}$.

3. The Efficiency of Temporary Capture by an Eccentric Planet

Now we estimate the dependences of the probability of temporary capture on $e_{\rm p}$ and $m_{\rm p}$ of the host planet. We define the probability as $K_{\rm tc}/K_{\rm enc}$, where $K_{\rm enc}$ and $K_{\rm tc}$ are the phase space volume that satisfies the conditions for encounters with the planet's Hill sphere, and that for temporary capture, respectively. Encounters with the Hill sphere are defined as those with minimum distance to the planet less than their instantaneous Hill radius $r_{\rm H}$. For simplicity, we here set $r_{\rm p} = a_{\rm p}(1 + e_{\rm p}^2/2)$. For example, we consider a close encounter orbit with $\bar{a} < 1$. The maximum eccentricity e_1 is

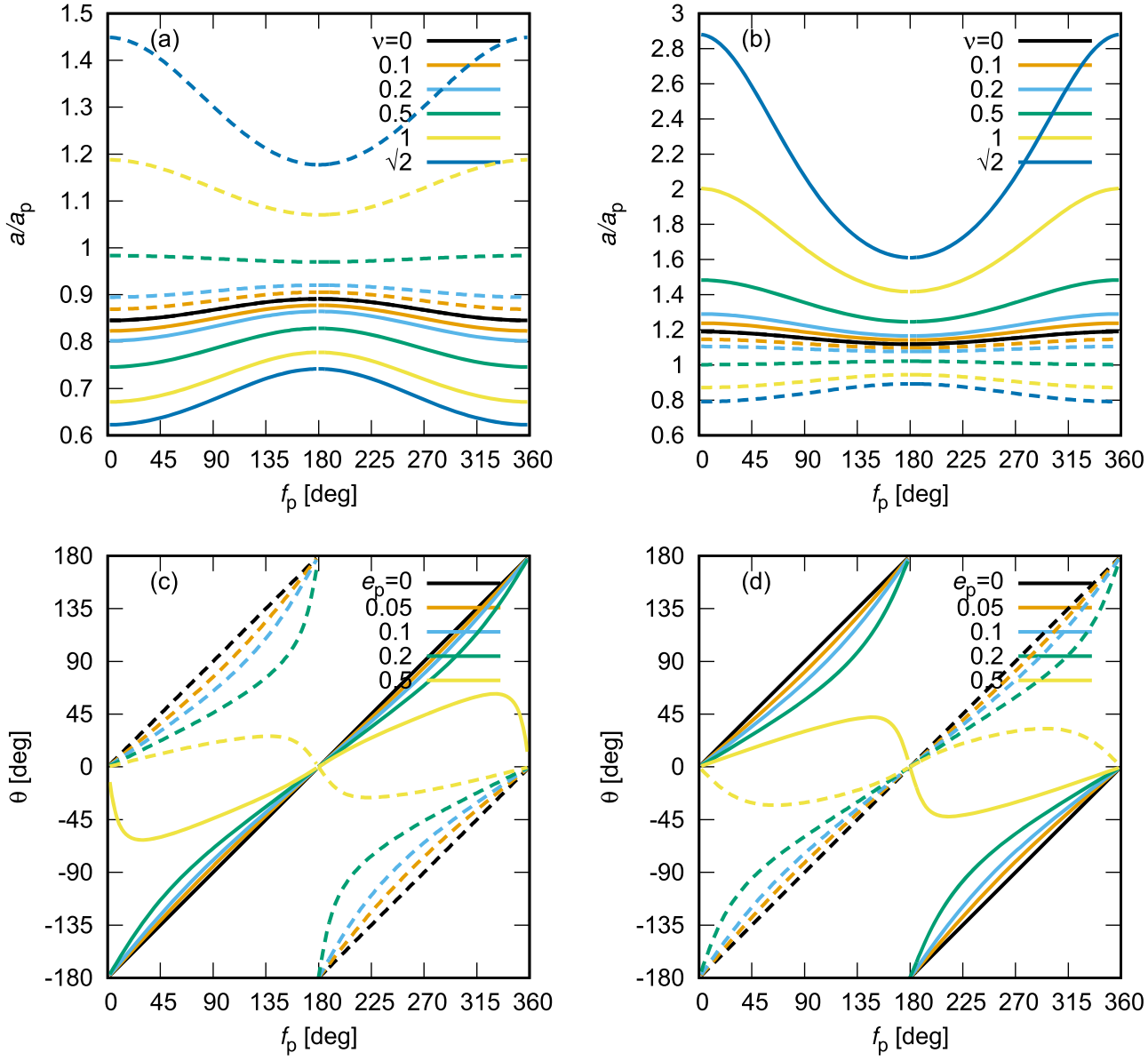

Figure 1. Solutions to Equations (16) are plotted against f_p with $e_p = 0.2$ and a Jovian mass planet for $\nu = 0$(black), 0.1 (orange), 0.2 (light blue), 0.5 (green), 1 (yellow), and $\sqrt{2}$ (blue): (a) L_1-type and (b) L_2-type captures. The solutions to Equations (19) with $\nu = \sqrt{2}$ and a Jovian mass planet are plotted for $e_p = 0$, 0.01, 0.02, 0.05, and 0.09: (c) L_1-type and (d) L_2-type captures. The solid and dashed curves are for prograde and retrograde captures, respectively.

required for an orbit with its aphelion at the L_2 point;

$$\bar{a}(1+e_1) = \left(1+\frac{1}{2}e_p^2\right)(1+\hat{r}_H) \to 1+e_1$$
$$= \left(1+\frac{1}{2}e_p^2\right)\left(\frac{1+\hat{r}_H}{\bar{a}}\right). \quad (24)$$

In a similar way, the minimum eccentricity e_2 satisfies

$$\bar{a}(1+e_2) = \left(1+\frac{1}{2}e_p^2\right)(1-\hat{r}_H) \to 1+e_2$$
$$= \left(1+\frac{1}{2}e_p^2\right)\left(\frac{1-\hat{r}_H}{\bar{a}}\right). \quad (25)$$

Then, the range of eccentricity for close encounters is given by

$$\Delta e = e_1 - e_2 = \left(1+\frac{1}{2}e_p^2\right)\frac{2\hat{r}_H}{\bar{a}}. \quad (26)$$

The range of eccentricity for close encounters with $\bar{a} > 1$ is the same. The range of the angle of perihelion for close encounters is $\Delta\theta/2\pi$, where we can set $\Delta\theta = 2\hat{r}_H$. Then we obtain K_{enc} as the phase space volume by integrating $\Delta e \cdot \Delta\theta/2\pi$ over $\bar{a}$ with the time weight ($\propto \bar{a}^{-3/2}$),

$$K_{enc} = \frac{\hat{r}_H}{\pi}\int_{\bar{a}_{min}}^{\bar{a}_{max}} \Delta e(\bar{a})\,\bar{a}^{-\frac{3}{2}}\,d\bar{a}$$
$$= \frac{2\hat{r}_H^2}{3\pi}\left(1+\frac{1}{2}e_p^2\right)\left(\bar{a}_{min}^{-\frac{3}{2}} - \bar{a}_{max}^{-\frac{3}{2}}\right), \quad (27)$$

where we assumed a uniform a-distribution of asteroids. We use $\bar{a}_{tc,min,L_1}$ and $\bar{a}_{tc,max,L_2}$ for $\bar{a}_{min}$ and $\bar{a}_{max}$, which are obtained from Equation (16). We set the upper limit of $\bar{a}_{max} = 3$ to avoid divergence in the calculation of K_{enc}. This is used only in cases of Jovian mass planets. Assuming $e_p \ll 1$ and $\hat{r}_H \ll 1$, one can find that $K_{enc} \propto \hat{r}_H^3$.

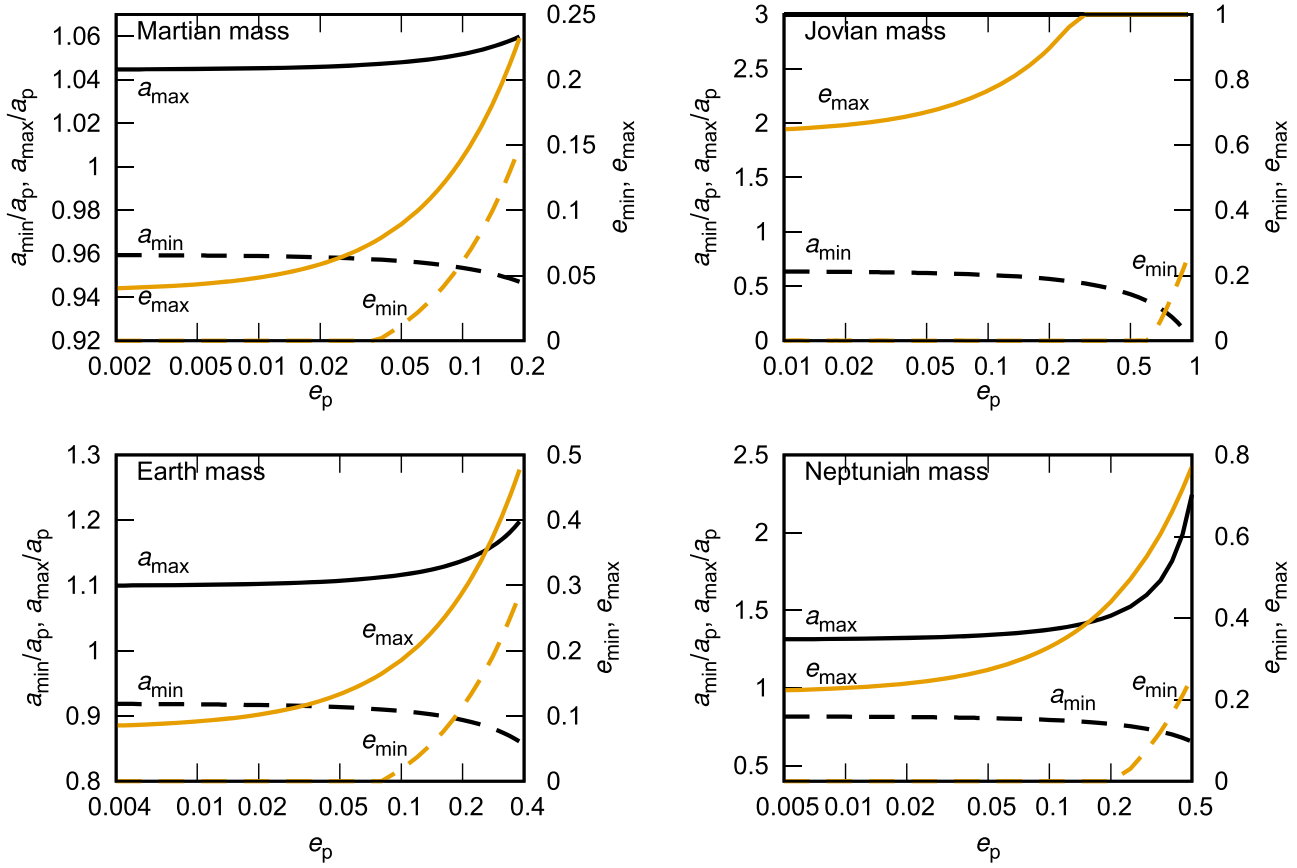

Figure 2. Ranges of initial orbital elements summarized for each planetary mass against e_p (top-left: Martian mass, top-right: Jovian mass, bottom-left: Earth mass, bottom-right: Neptunian mass.) Black curves show $\bar{a}_{max}$ (solid) and $\bar{a}_{min}$ (dashed) on the left y-axis and orange curves show e_{max} (solid) and e_{min} (dashed) on the right y-axis.

The phase space volume for temporary capture is much more restricted than for the encounters. In a similar way as we defined K_{enc}, the phase volume of temporary capture is given by

$$K_{tc} = \frac{1}{T_p}\int_0^{T_p}\int_{\bar{a}_{min}}^{\bar{a}_{max}} \Delta e_{tc}\,\frac{\Delta\theta_{tc}}{2\pi}\,\bar{a}_{tc}^{-\frac{3}{2}}\,d\bar{a}_{tc}\,dt. \tag{28}$$

Because a_{tc}, e_{tc}, and θ_{tc} are correlated, it is useful to rewrite Δe_{tc}, $\Delta\theta_{tc}$, and da_{tc} as $\Delta e_{tc} = (de_{tc}/d\nu_{tc})\Delta\nu_{tc}$, $\Delta\theta_{tc} = (d\theta_{tc}/d\nu_{tc})\hat{r}_H\Delta\nu_{tc}$, and $d\bar{a}_{tc} = (d\bar{a}_{tc}/d\nu_{tc})d\nu_{tc}$. Using these relations, we change the integral of K_{tc} by da_{tc} to that by $\Delta\nu_{tc}$. For $e_p = 0$, we set $\Delta\theta_{tc} = \Delta\gamma\cdot\hat{r}_H$, where $\Delta\gamma \ll 1$. Because the integrands depend on f_p, we also added time averaging over an orbital period of the planet ($T_p = 1$).

Thereby, the temporary capture rate is given from Equations (16) as

$$K_{tc} = \frac{(\Delta\nu)^2\hat{r}_H}{2\pi T_p}\int_0^{T_p}\int_{\nu_{min}}^{\nu_{max}} \frac{de_{tc}}{d\nu_{tc}}\frac{d\theta_{tc}}{d\nu_{tc}}\frac{d\bar{a}_{tc}}{d\nu_{tc}}\,\bar{a}_{tc}^{-\frac{3}{2}}\,d\nu_{tc}\,dt, \tag{29}$$

$$\frac{d\bar{a}_{tc}}{d\nu} = \pm 2\frac{\bar{a}_{tc}^2}{\Phi_p}\sqrt{3}\,\hat{r}_H\left(\sqrt{2-\Phi_p} \pm \sqrt{3}\,\hat{r}_H\nu\right) \tag{30}$$

$$\frac{de_{tc}}{d\nu} = \frac{de_{tc}}{d\bar{a}_{tc}}\frac{d\bar{a}_{tc}}{d\nu} \tag{31}$$

$$\frac{d\theta_{tc}}{d\nu} = \frac{\frac{dg}{d\nu}}{\sqrt{1-g^2}} \tag{32}$$

$$\frac{de_{tc}}{d\bar{a}_{tc}} = \Phi_p A_{\mp}\sin^2\alpha_p\left(1-\frac{\Phi_p A_{\mp}}{\bar{a}_{tc}}\right)\bar{a}_{tc}^{-2}e_{tc}^{-1} \tag{33}$$

$$\frac{dg}{d\nu} = \frac{dg}{de_{tc}}\frac{de_{tc}}{d\nu};\quad \frac{dg}{de_{tc}} = -ge_{tc}^{-1} \pm \frac{\sin\alpha_p}{\sqrt{e_{tc}^2-\cos^2\alpha_p}}. \tag{34}$$

For $e_p = 0$,

$$K_{tc} = \frac{\Delta\nu\Delta\gamma\hat{r}_H}{2\pi}\int_{\nu_{min}}^{\nu_{max}}\frac{de_{tc}}{d\nu_{tc}}\frac{d\bar{a}_{tc}}{d\nu_{tc}}\,\bar{a}_{tc}^{-\frac{3}{2}}\,d\nu_{tc}. \tag{35}$$

Assuming $e_p \ll 1$ and $\hat{r}_H \ll 1$, one can find $(da_{tc}/d\nu_{tc}) \propto \hat{r}_H$, and $(de_{tc}/d\bar{a}_{tc})$, (dg/de_{tc}), and g are independent of $\hat{r}_H$. This leads to $K_{tc} \propto \hat{r}_H^3$, which is the same as K_{enc}, implying that K_{tc}/K_{enc} is independent of m_p for $e_p \ll 1$.

The integration range, $\nu_{min} < \nu_{tc} < \nu_{max}$, can be simply estimated in the framework of the two-body problem (planet–particle) as follows. The physical radius of the planet may give the value of ν_{min}. A planetocentric temporarily captured orbit has its apocenter distance at $a_s(1+e_s) \simeq r_H$. The pericenter distance, $a_s(1-e_s)$, must be larger than the physical radius of the planet, R_p, to avoid a collision. From these two equations,

$$e_s < \frac{1-(R_p/r_H)}{1+(R_p/r_H)} \tag{36}$$

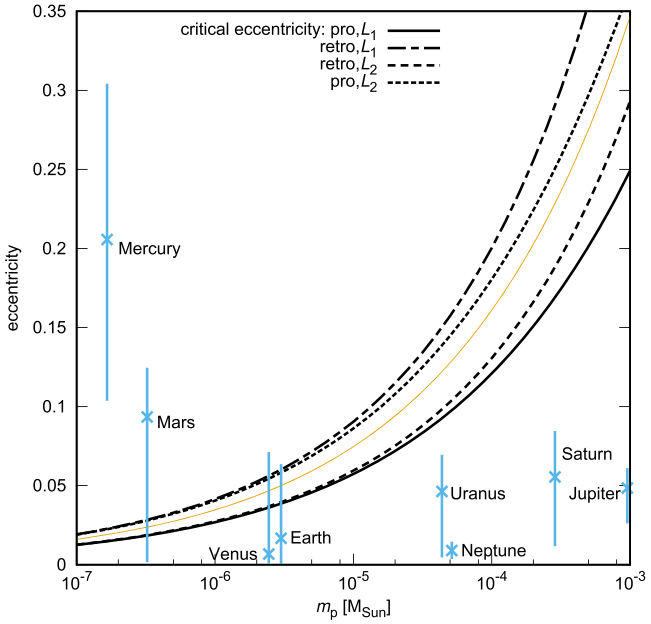

Figure 3. Critical eccentricity e_p^c for $\nu = \sqrt{2}$ plotted against m_p. The curve types indicate the capture type (solid: [prograde, L_1], long-short dashed: [retrograde, L_1], dashed: [retrograde, L_2], short dashed: [prograde, L_2]). The orange curve shows $e_p = 5\hat{r}_H$. Current eccentricities of eight planets of the solar system are also plotted against their mass. The error bars show the variations over 10 Myr calculated following Laskar (1988).

Since $\nu = \sqrt{\kappa} = \sqrt{1 - e_s}$ for $f_s = 0$,

$$\nu_{\min} = \sqrt{\frac{R_p/r_H}{1 + (R_p/r_H)}} \simeq \sqrt{R_p/r_H}. \quad (37)$$

The simplest assumption for the maximum value in the framework of the two-body problem is $\nu_{\max} = \sqrt{2}$, which is the upper limit for an elliptic orbit around the planet. However, the effect of the third body (the Sun) changes them. We found that it is more appropriate to assume $\nu_{\min} = 0.25$ and $\nu_{\max} = 2$ for a prograde trap and $\nu_{\min} = 0.5$ and $\nu_{\max} = \sqrt{2}$ for a retrograde trap from the orbital calculations described below. We adopt these integration ranges.

Figure 4 shows the ratio K_{tc}/K_{enc} as a function of e_p for planets with Martian, Jovian, Earth, and Neptunian mass. Each plot has four curves for the temporary capture types, and the sum of the four types (the black line). The total ratio (black) is almost constant or gradually increases with e_p until e_p exceeds e_p^c. The asymptotic values of K_{tc}/K_{enc} at $e_p \to 0$ are independent of planetary mass (m_p) and semimajor axis (a_p), as we predicted. As shown in Figure 4, $e_p^c \simeq 5\hat{r}_H$ where $\hat{r}_H = 4.8 \times 10^{-3}$ for Mars, $\hat{r}_H = 0.068$ for Jupiter, $\hat{r}_H = 0.01$ for Earth, and $\hat{r}_H = 0.026$ for Neptune. For $e_p > e_p^c$s, K_{tc} decays with e_p approximately $\propto e_p^{-1}$. As will be shown in the next section, the functional form of the predicted K_{tc}/K_{enc} agrees very well with the results of numerical orbital integrations, while the allowance for temporary capture $\Delta\nu$ and $\Delta\gamma$ cannot be estimated by analytical arguments here. Because ν expresses the satellite orbital energy at the Hill radius, it is expected that the allowance $\Delta\nu$ is independent of m_p and a_p as well. Also the independence of $\Delta\gamma$ is expected since the angle $\Delta\theta_{tc}$ would be a function only of $\hat{r}_H$. From comparison with numerical simulations, we empirically set $\Delta\nu \sim 0.025$ and $\Delta\gamma \sim 0.05$.

4. Comparison with Numerical Results

We perform numerical calculations for the temporary capture of bodies by planets with Mars, Jupiter, Earth, and Neptune masses to evaluate the relevance of our analytical formulae.

4.1. Methods and Initial Conditions

We compute the orbital evolution of massless bodies, which correspond to asteroids, perturbed by a planet in a circular or eccentric orbit, using a fourth-order Hermite integration scheme. The parameters are summarized in Table 1. The number of massless bodies in each run is 5×10^6. Asteroids are initially uniformly distributed on the a, e-plane between $\bar{a}_{tc,min,L_1} < \bar{a} < \bar{a}_{tc,max,L_2}$, $e_{min} < e < e_{max}$, which are derived analytically and numerically in Section 2.3.2 and summarized in Figure 2. The parameter θ is also uniformly distributed between 0 and 2π. We set the upper limit of $\bar{a}_{tc,max,L_2} = 3$. In most runs we assume $i = 0$ for the asteroids. In several additional runs, we give i with a uniform distribution for $0 < i < i_{tc,max}$ where $i_{tc,max}$ is given by Equation (23) for $f_p = 180^\circ$ and $\nu = \sqrt{2}$. We regard asteroids as temporarily captured bodies if they stay within r_H from the planet longer than one orbital period T_p.

Using the planetocentric location and the relative velocity vector to the planet, at the moment when an asteroid enters the r_H region around the planet for the first time, we define the type of temporary capture: [prograde-L_1], [retrograde-L_1], [retrograde-L_2], and [prograde-L_2].

In this paper, we focus on the equilibrium state where the ratio of temporary capture and encounter rates becomes constant with time. To obtain this state, we first perform several long-time calculations with 10^5 particles for $10^5 T_p$ and choose the time range where the ratio is constant with time. Note that Higuchi & Ida (2016) presented the cumulative number of captured bodies over 10^6 years, which is not directly compared with the results presented here.

4.2. Results

Figure 5 shows θ of the temporarily captured bodies against f_p for a Martian mass planet with various e_p. The analytical prediction (Equation (19)) for $0 \leqslant \nu \leqslant \sqrt{2}$ is also plotted. The analytical prediction, which determines the critical eccentricity for temporary capture (e_p^c), agrees well with the numerical results.

Figure 6 shows the ratio (n_{tc}/n_{enc}) of the temporary capture and encounter rates as a function of e_p for planets with Martian, Jovian, Earth, and Neptunian masses. The ratio drops beyond the predicted values of $e_p^c \simeq 5\hat{r}_H$, which are 0.02, 0.27, 0.04, and 0.1 for Martian, Jovian, Earth, and Neptunian mass respectively. This drop of n_{tc}/n_{enc} is well reproduced by the analytical prediction in Figure 4.

The value of n_{tc}/n_{enc} for $e_p < e_p^c$ is $\sim 10^{-3}$, which is almost independent of the planetary mass, as predicted. We performed additional numerical calculations using particles with $i < i_{max}$ for $\nu = \sqrt{2}$ given by Equation (23). The results show that the values of n_{tc}/n_{enc} for the 3D calculations are similar to those for the 2D calculations (within a factor of 2).

5. Summary and Discussion

In order to explore the origins of irregular or minor satellites around the planets in the solar system, we have investigated the probability of temporary capture through semi-analytical

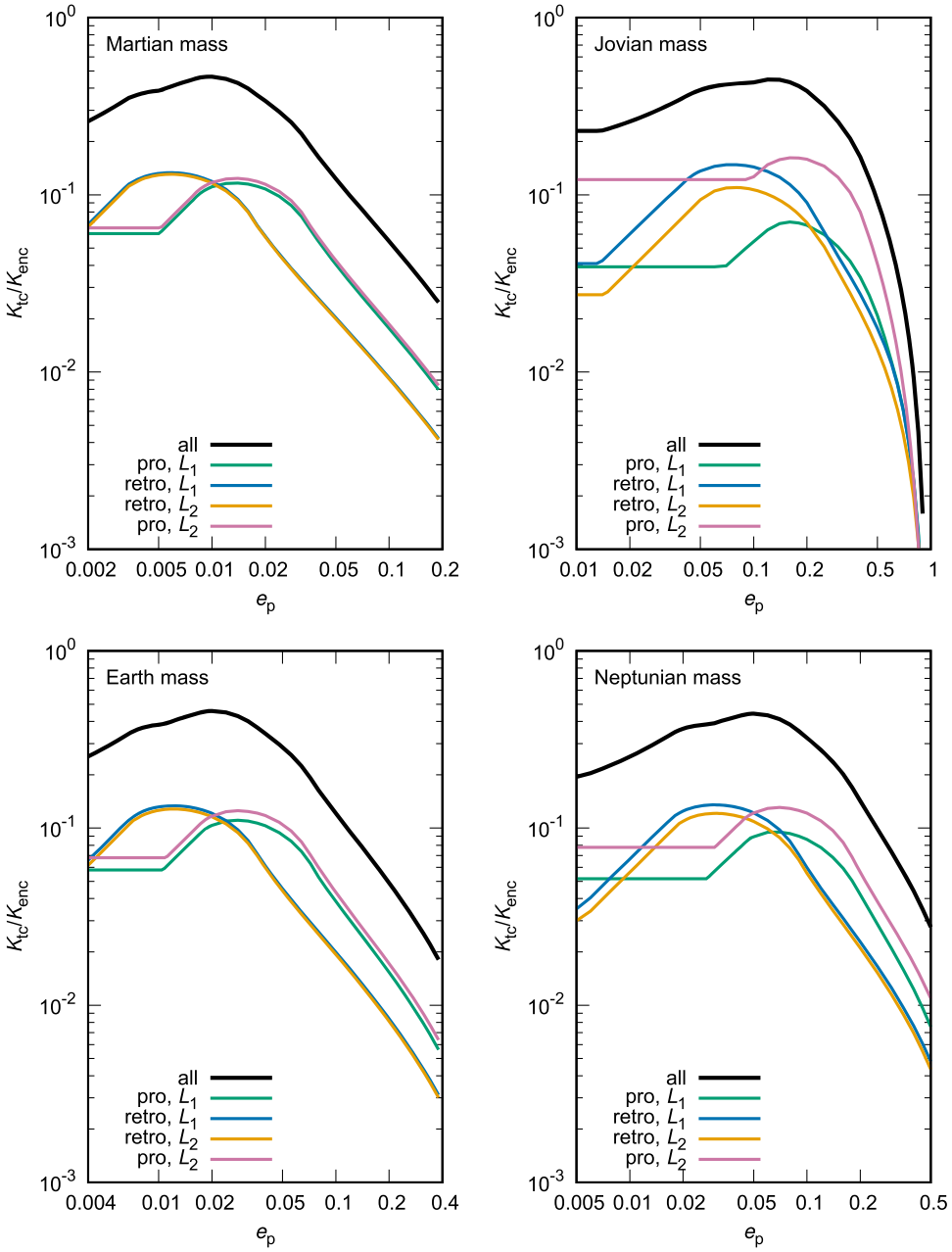

Figure 4. Efficiency of temporary capture K_{tc}/K_{enc} plotted against e_p for planets with Martian (top-left), Jovian (top-right), Earth (bottom-left), and Neptunian (bottom-right) mass using $\nu_{min} = 0.25$ and $\nu_{max} = 2$ for prograde and $\nu_{min} = 0.5$ and $\nu_{max} = \sqrt{2}$ for retrograde. We set $\Delta\nu \sim 0.025$ and $\Delta\gamma \sim 0.05$. The K_{tc} for each temporary capture type is plotted in color; [prograde, L_1] (green), [retrograde, L_1] (blue), [retrograde, L_2] (orange), and [prograde, L_2] (pink). The black curve shows the sum of the four types. We adopt Equation (35) for K_{tc} if K_{tc} with Equation (29) for $e_p < e_p^c$ is less than that with Equation (35).

Table 1
Parameters of Planets Used in Numerical Calculations

Planet	a_p (au)	m_p ($M_\odot$)	e_p Range
Earth	1	3.00e–06	0.004–0.36
Mars	1.52	3.72e–07	0.002–0.18
Jupiter	5.2	9.55e–04	0.01–0.9
Neptune	30.1	5.15e–05	0.005–0.5

arguments and numerical integration. We extended the analysis of temporary capture around a planet in a circular orbit developed by Higuchi & Ida (2016) to that around a planet in an eccentric orbit, allowing us to discuss the origins of the Martian satellites. We derived the capture probability as a function of planetary mass (m_p) and eccentricity (e_p). Analytical formulae reproduce the numerical integrations very well.

We found that temporary capture occurs at ∼0.1% of encounters that enter Hill sphere of a planet, independent of m_p, a_p (semimajor axis) and e_p up to a critical value $e_p^c \simeq 5(m_p/3M_\odot)^{1/3}$. For $e_p > e_p^c$, the probability decays with increasing e_p as $\propto e_p^{-(1-2)}$.

The current eccentricity of Mars is several times larger than e_p^c, so that the capture origin of Phobos and Deimos looks unfavored. However, as shown in Figure 3, the Martian eccentricity changes with time and can be lower than e_p^c for some fraction of time, and temporary capture may have been

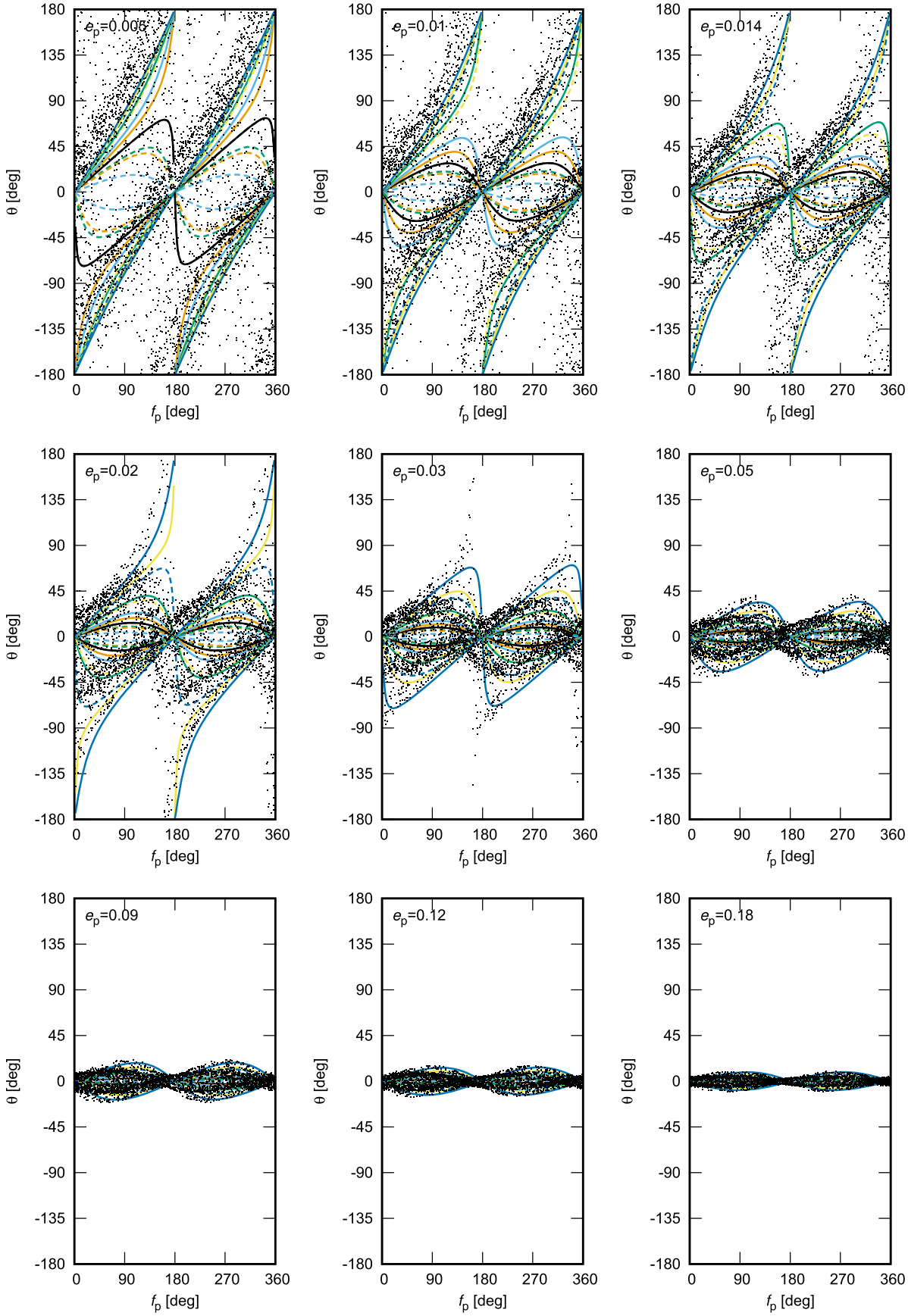

Figure 5. Argument of perihelion of temporarily captured bodies by a Martian mass planet with various e_p at the moment of entering the Hill sphere for the first time plotted against f_p. The solutions to Equation (19) for each temporary capture type for $\nu = 0$(black), 0.1 (orange), 0.2 (light blue), 0.5 (green), 1 (yellow), and $\sqrt{2}$(blue) are also plotted. Solid and dashed curves are for prograde and retrograde temporary capture, respectively. All types of temporary capture are plotted in the same panel.

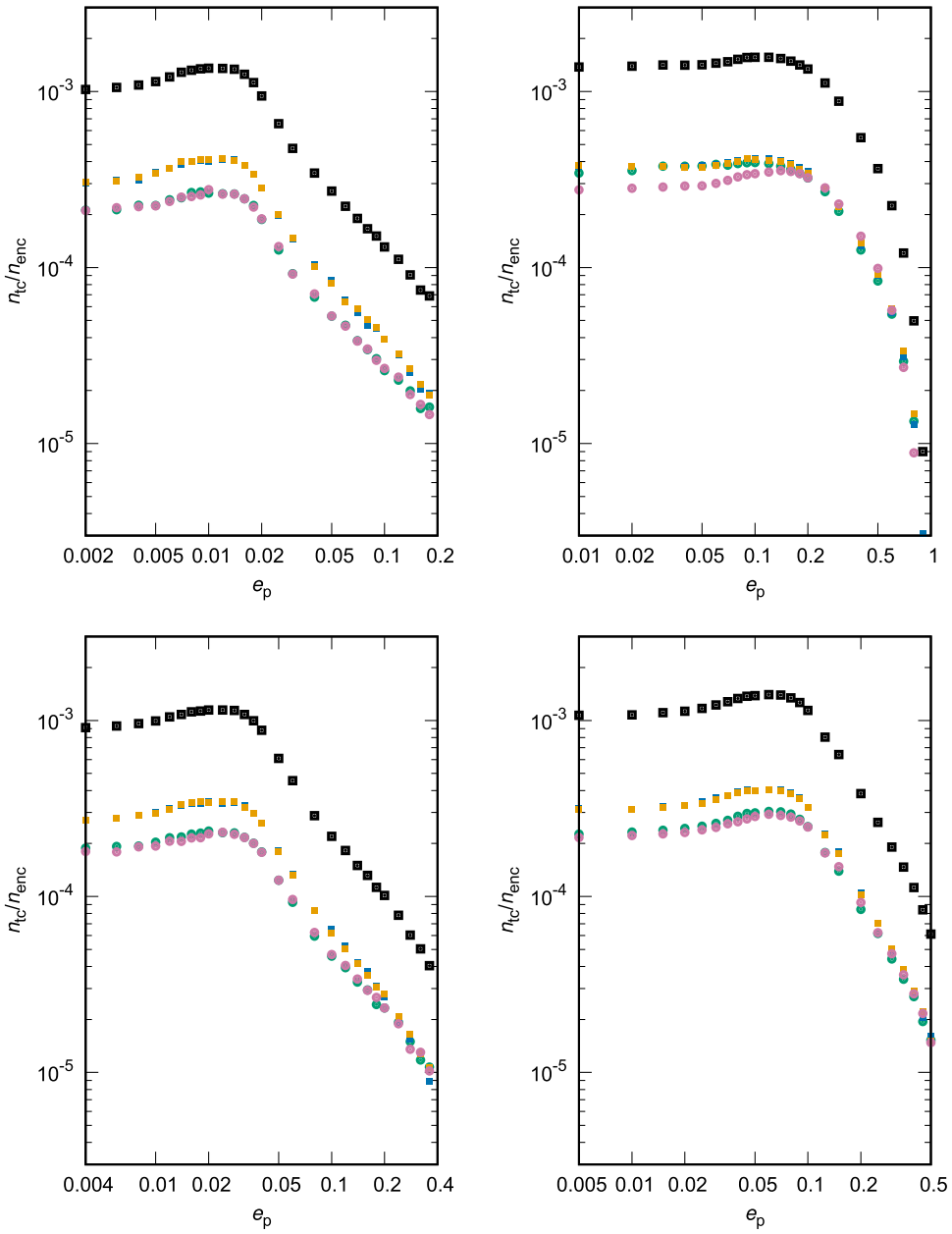

Figure 6. Ratio of the number of temporary captures n_{tc} to that of encounters n_{enc} plotted against e_p for planets with Martian (top-left), Jovian (top-right), Earth (bottom-left), and Neptunian (bottom-right) mass. The colors indicate the types of temporary capture; [prograde, L_1] (green), [retrograde, L_1] (blue), [retrograde, L_2] (orange), [prograde, L_2] (pink), and the sum of all types (black).

available in the past. Note again that temporary capture is a necessary condition for permanent capture and their respective probabilities are not necessarily proportional to each other. As will be discussed in a separate paper, tight capture could be found in the cases where $e_p > e_p^c$. In a subsequent paper, we will discuss the probability of permanent capture and the possibility of the capture origin of Phobos and Deimos.

We thank an anonymous referee for his/her useful comments that helped to improve the paper. This work was supported by JSPS KAKENHI grant Number 23740335 and 15H02065. Data analyses were in part carried out on the PC cluster at the Center for Computational Astrophysics, National Astronomical Observatory of Japan.

References

Burns, J. A. 1978, in Symp. On the Satellites of Mars, Vistas in Astronomy, Vol. 22 (Hampton, VA: STI), 193
Citron, R. I., Genda, H., & Ida, S. 2015, Icar, 252, 334
Fraeman, A. A., Murchie, S. L., Arvidson, R. E., et al. 2014, Icar, 229, 196
Higuchi, A., & Ida, S. 2016, AJ, 151, 16
Ito, T., Masuda, K., Hamano, Y., & Matsui, T. 1995, JGR, 100, 15147
Jewitt, D., & Haghighipour, N. 2007, ARA&A, 45, 261
Laskar, J. 1988, A&A, 198, 341
Murray, C. D., & Dermott, S. F. 1999, Solar System Dynamics (Cambridge: Cambridge Univ. Press)
Nicholson, P. D., Ćuk, M., Sheppard, S. S., Nesvorný, D., & Johnson, T. V. 2008, in The Solar System Beyond Neptune, Vol. 411, Irregular Satellites of the Giant Planets, ed. M. A. Barucci et al. (Tucson, AZ: Univ. Arizona Press), 411
Rosenblatt, P., Charnoz, S., Dunseath, K. M., et al. 2016, NatGe, 9, 581
Roy, A. E. 2005, Orbital Motion (4th ed.; Boca Raton, FL: CRC Press)